Ultra-Wideband Analog-to-Digital Conversion Via Signal Expansion

Sebastian Hoyos, *Member, IEEE,* and Brian M. Sadler, *Senior Member, IEEE*

(Invited Paper)

***Abstract*—We consider analog to digital (A/D) conversion, based on the quantization of coefficients obtained via the projection of a continuous time signal over a set of basis functions. The framework presented here for A/D conversion is motivated by the sampling of an input signal in domains which may lead to significantly less demanding A/D conversion characteristics, i.e., lower sampling rates and lower bit resolution requirements. We show that the proposed system efficiently parallelizes the analog to digital converter (ADC), which lowers the sampling rate requirements by increasing the number of basis functions on which the continuous time signal is projected, leading to a tradeoff between sampling rate reduction and system complexity. Additionally, the A/D conversion resolution requirements can be reduced by optimally assigning the available number of bits according to the variance distribution of the coefficients obtained from the signal projection over the new A/D conversion domain. In particular, we study A/D conversion in the frequency domain, where samples of the continuous signal spectrum are taken such that no time aliasing occurs in the discrete time version of the signal. We show that the frequency domain ADC overcomes some of the difficulties encountered in conventional time-domain methods for A/D conversion of signals with very large bandwidths, such as ultra-wideband (UWB) signals. The proposed A/D conversion method is compared with conventional ADCs based on pulse code modulation (PCM). Fundamental figures of merit in A/D conversion and system tradeoffs are discussed for the proposed ADC. The signal-to-noise and distortion ratios of the frequency domain ADC are presented, which quantify the impact of the most critical impairments of the proposed ADC technique. We also consider application to communications receivers, and provide a design example of a multi-carrier UWB receiver.**

***Index Terms*—Analog to digital conversion (ADC), communications receiver, high-speed ADC, mixed-signal processing, quantization, signal expansion, ultra-wideband.**

I. Introduction

DIGITAL ULTRA-WIDEBAND (UWB) systems are highly desirable, offering flexibility and programmability. However, while system data rates and bandwidths continue to expand, analog-to-digital converters (ADCs) are limited in bandwidth, resolution, and power consumption [1]. Currently available architectures used in the fabrication of ADCs include the *flash* architecture, which is based on parallel techniques that use $2^b - 1$ comparators to achieve b bits of resolution. All comparators sample the analog input signal simultaneously, making the flash ADC inherently fast. Because of the parallelism of this architecture, the number of comparators grows exponentially with b, thus increasing the power consumption and also the circuitry area. This in turn increases the input capacitance limiting the system bandwidth and makes it difficult to match components. Some variations of the flash architecture such as the folded-flash [2]–[4], pipelined [5], [6], and time interleaved [7] architectures have been proposed in order to overcome some of these problems. Among the difficulties that have slowed the evolution of ADCs is the aperture jitter or aperture uncertainty, which is the sample-to-sample variation of the instant in time at which sampling occurs. Moreover, the speed of sampling is limited by the frequency characteristic of the device used in the design, which limits the ability of the comparators to make an unambiguous decision about the input voltage.

To overcome these problems, techniques that aim to relax the operational conditions of the ADC have been proposed. Low-resolution ADC is possible with sigma-delta modulation [8]. The noise penalty associated with the use of a few bits or less in the quantization process is overcome in the sigma-delta scheme by using either signal oversampling or multi-band processing techniques [9], [10]. In particular, when a single bit is used, the implementation is greatly simplified and practical mono-bit UWB digital communications receivers have significant potential [11]–[13]. These techniques generally require sampling at or above the Nyquist rate over the full signal bandwidth, and so suffer from the aforementioned high speed issues. In addition, they provide a single UWB serial data stream, which may stress the digital signal processing following the ADC.

An alternative is to channelize the analog signal by means of a bank of bandpass filters [14], and the output of each filter are sampled in parallel. Multirate approaches may also be used [15]. ADC thus occurs at a reduced rate for each of the resultant bandpass signals. The bandpass outputs may also be frequency translated to baseband [16], allowing the use of a single lowpass filter design. However, the bandpass analog filter bank design is difficult, and the resulting nonideal filters cause signal leakage across the bands that can degrade overall system performance unless properly accounted for. The design of analog filters with sharp rolloff needed in the multiband ADC approaches also suffers from power consumption and a large circuitry area to accommodate the passive elements (i.e., inductors and capacitors).

In this paper, we consider an alternative parallel sampling scheme. Our approach is to project the signal over basis

Manuscript received February 16, 2005; revised April 20, 2005. The review of this paper was coordinated by Prof. R. Qiu.

S. Hoyos is with the Berkeley Wireless Research Center, Department of Electrical Engineering and Computer Sciences, University of California, Berkeley, Berkeley, CA 94704-1302 (e-mail: hoyos@eecs.berkeley.edu).

B. M. Sadler is with the Army Research Laboratory, AMSRD-ARL-CI-CN, Adelphi, MD 20783 (e-mail: bsadler@arl.army.mil).

Digital Object Identifier 10.1109/TVT.2005.856195

functions, and then sample the basis coefficients. Representing the signal in a domain other than the classical time-domain sampling approach yields parallel data streams, and potentially improves the distortion versus average bit rate in the sampled output. The time-domain signal may be reconstructed via a linear digital computation, or signal processing can be carried out directly with the basis coefficients. N basis coefficients are calculated in a parallel analog computation every T_c seconds, followed by N parallel ADCs. Thus, the ADCs run at a speed that is inversely proportional to the time-window duration T_c, which can be properly designed to meet the speeds allowed by the technology used in the implementation. The speed reduction comes at the cost of the implementation of the local basis function generators, mixers, and integrators needed to project the continuous-time signal onto the set of basis functions. This introduces a tradeoff between sampling speed reduction and system complexity that is characterized in this paper. Although similar reductions in the speed of the quantizers could be achieved in the time domain by using a time-interleaved bank of quantizers [7], [17], [18], synchronization problems, the very fine time resolution in high-speed applications, and the fact that all the ADCs see the full bandwidth of the input signal makes it difficult to design the sample/hold circuitry, and causes the overall design to require significant power. In addition, the signal expansion approach avoids the sharp-rolloff filter bank needed in multiband ADC architectures. Mixing with basis functions, followed by integration over a time window required to project the signal, generally synthesizes a filter bank with overlapping spectrum and smooth transitions. The relaxed implementation requirements are a key motivation for the ideas presented here.

Potential lower bit requirements, or equivalently, the potential improvement in the distortion of the ADC of signal expansions, can be achieved by optimally allocating the available number of bits in the quantization of the coefficients obtained through the projection of the continuous-time signal over the basis set. The possibility of efficiently allocating the available resources in terms of number of bits per sample is a feature that is not available in conventional time domain ADC. Optimal bit allocation is possible in the proposed A/D conversion scheme because some signal characteristics that are hidden in the time-domain, such as power spectral distribution, can now be explored by projecting the continuous-time signal.

As a particular case, we consider A/D conversion in the frequency domain [19]–[21], in which samples of the signal transform are taken at a rate that guarantees no aliasing in the discrete-time signal domain. The discrete frequency samples are then quantized by a set of quantizers operating over DC levels that change with a rate that is much lower than the Nyquist rate needed in the sampling of the time domain signal. Other domains, such as those provided by the Hadamard, Walsh, Walsh–Fourier, and Haar wavelet transforms, are also potential candidates.

Although the representation of an analog signal through its projection on basis functions is a well known continuous signal processing tool, its specific application in A/D conversion has not been fully investigated. Basic theoretical aspects and practical issues in A/D conversion have not been reported in the literature, to the best of the authors' knowledge. Perhaps, the closest related publication is sampling of signal projections [22], and some information theory work on overcomplete expansions [23], [24], where quantization of the coefficients of redundant expansions is carried out. These publications study improved sampling techniques based mainly on vector quantization, oversampling [25], [26], and signal reconstruction algorithms.

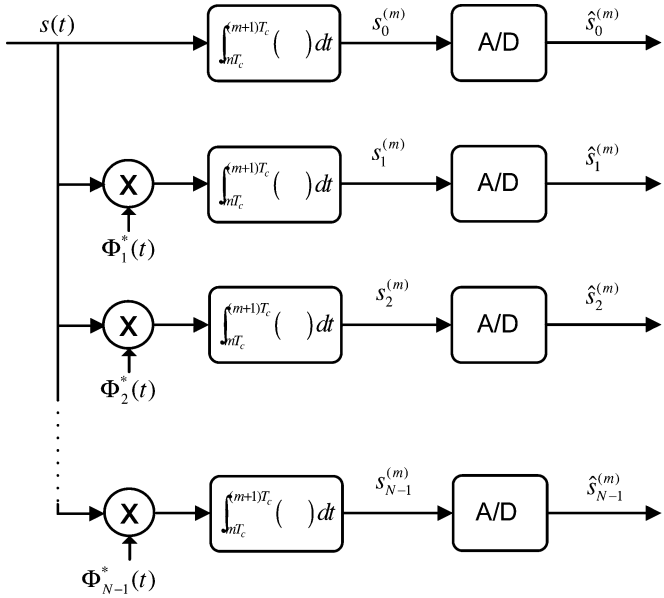

Fig. 1. Block diagram of the analog-to-digital converter, which expands the received signal using a set of basis functions.

The paper is organized as follows. Section II sets up the signal expansion and sampling ideas. In Section III, we provide an MSE distortion analysis, including quantization effects and truncation of the number of basis coefficients N, and compare these results with conventional time domain ADCs. We also consider optimum bit allocation under a distortion metric, illuminating tradeoffs involving complexity (choice of N) and number of bits used in quantization. In Section IV, we describe the application to communications systems, and illustrate how a low complexity receiver operates with the sampled basis coefficients. Section V focuses on the use of a Fourier basis, and gives the specifics of spectral sampling. In Section VI we provide an SNR analysis of the Fourier-basis ADC operating with imperfect devices, including errors in gain, timing, and frequency offset. Finally, in Section VII we briefly consider application to UWB multicarrier systems, and Section VIII provides conclusions.

II. Analog to Digital Conversion of Signal Expansions

The block diagram depicted in Fig. 1 shows the basic signal expansion principle of the proposed A/D conversion. The received signal $s(t)$ is decomposed every T_c seconds into N components which are obtained through the projection over the basis $\Phi_l(t)|_{l=0}^{N-1}$. The coefficients $s_l^{(m)}|_{l=0}^{N-1}$ are found as

$$s_l^{(m)} = \langle s(t), \Phi_l(t) \rangle_{m,T_c} = \int_0^{T_c} s(t + mT_c)\Phi_l^*(t)\,\mathrm{d}t. \quad (1)$$

If the mean square error (MSE) criterion is used to reconstruct the received signal $s(t)$ in the interval $mT_c \le t \le (m+1)T_c$

through a linear combination of the basis functions $\Phi_l(t)|_{l=0}^{N-1}$, in general the coefficients $s_l^{(m)}|_{l=0}^{N-1}$ will have to be linearly transformed. We define the $N \times N$ matix Ψ, which contains the correlation coefficients of the basis functions,

$$\begin{aligned}\psi_{n,l} &= \langle \Phi_n(t), \Phi_l(t) \rangle_{T_c} \\ &= \int_0^{T_c} \Phi_n^*(t)\Phi_l^*(t)\,\mathrm{d}t, \quad n,l = 0,\ldots,N. \end{aligned} \tag{2}$$

The coefficients $a_l^{(m)}$ that provide the best MSE approximation are found by solving the linear equation

$$s^{(m)} = \Psi\, a^{(m)} \tag{3}$$

where the vectors $s^{(m)}$ and $a^{(m)}$ are defined as, $s^{(m)} = [s_0^{(m)} \cdots s_{N-1}^{(m)}]^T$ and $a^{(m)} = [a_0^{(m)} \cdots a_{N-1}^{(m)}]^T$. Solving (3) requires invertibility of the matrix Ψ. If the basis functions are orthonormal, then $a^{(m)} = s^{(m)}$. The best MSE approximation is given by

$$\tilde{s}^{(m)}(t) = \sum_{l=0}^{N-1} a_l^{(m)} \Phi_l(t), \quad 0 \le t \le T_c \tag{4}$$

where the signal $\tilde{s}^{(m)}(t), 0 \le t \le T_c$, is the best MSE approximation of the input signal $s(t), mT_c \le t \le (m+1)T_c$. At the end of the conversion time T_c, the coefficients $s_l^{(m)}|_{l=0}^{N-1}$ reach a constant value that is fed to a set of quantizers $Q_l^{(m)}|_{l=0}^{N-1}$, one for each coefficient, which return the digital words $\hat{s}_l^{(m)}|_{l=0}^{N-1}$. The lth quantizer $Q_l^{(m)}$ has 2^{b_l} output levels, where $b_l|_{l=0}^{N-1}$ is the number of bits used to obtain the quantized set of coefficients $\hat{s}_l^{(m)}|_{l=0}^{N-1}$. These values represent the output of the analog to digital converter for the input signal in a T_c second interval. Notice that the signal $s(t)$ is being segmented by a rectangular window for simplicity; windows with preferable characteristics can be used instead. The number of coefficients N used in the A/D conversion is intimately related to the conversion time T_c, and will affect the degree of the approximation indicated in (4), up to the point where the signal $s(t)$ is represented with zero error energy with a sufficient number of coefficients[1] N_*. When only a limited number of coefficients ($N \le N_*$) is used in the A/D signal conversion, some distortion is introduced. This distortion, plus the distortion introduced in the quantization process, constitutes the major sources of distortion in the proposed A/D conversion, and is analyzed in Section III. We also consider timing and frequency offset distortion in Section VI.

[1]The existence of the number N_* that makes the mean square error zero assumes that the basis functions $\Phi_l(t)|_{l=0}^{N_*-1}$ span the input signal $s(t)$. It is also possible that N_* tends to infinity as, for example, happens with signals with infinite spectral support (non-bandlimited signals) when they are projected in the frequency domain. However, for simplicity in the analysis, it is assumed that the input signal $s(t)$ is a smooth, well behaved signal (ideally a bandlimited signal) that can be represented with a finite number of coefficients N_*. The particular conditions that $s(t)$ must satisfy for the existence of N_* will depend on the domain chosen for the A/D conversion.

III. ADC Distortion With an Orthogonal Basis due to Limited Number of Coefficients and Quantization Error

Without loss of generality, consider the interval $0 \le t \le T_c$, in which the coefficients $\hat{a}_l|_{l=0}^{N-1}$ at the output of the A/D converter provide a representation of the analog input signal in the conversion time T_c. The reconstructed signal is expressed as

$$\hat{s}(t) = \sum_{l=0}^{N-1} \hat{a}_l \Phi_l(t), \quad 0 \le t \le T_c. \tag{5}$$

Using the MSE criterion, the total distortion D can be expressed as

$$\begin{aligned} D &= E\{|s(t) - \hat{s}(t)|^2\} \\ &= E\{(s(t) - \hat{s}(t))(s(t) - \hat{s}(t))^*\} \\ &= E\left\{\left|\sum_{l=0}^{N_*-1} a_l\Phi_l(t) - \sum_{l=0}^{N-1} \hat{a}_l\Phi_l(t)\right|^2\right\} \\ &= E\left\{\left|\sum_{l=N}^{N_*-1} a_l\Phi_l(t) + \sum_{l=0}^{N-1} a_l\Phi_l(t) - \sum_{l=0}^{N-1} \hat{a}_l\Phi_l(t)\right|^2\right\} \\ &= E\left\{\left|\sum_{l=N}^{N_*-1} a_l\Phi_l(t)\right|^2\right\} + E\left\{\left|\sum_{l=0}^{N-1} (a_l - \hat{a}_l)\Phi_l(t)\right|^2\right\} \\ &\quad + \sum_{l=N}^{N_*-1}\sum_{k=0}^{N-1} E\{a_l^*(a_k - \hat{a}_k)\}\Phi_l^*(t)\Phi_k(t) \\ &\quad + \sum_{l=N}^{N_*-1}\sum_{k=0}^{N-1} E\{a_l(a_k^* - \hat{a}_k^*)\}\Phi_l(t)\Phi_k^*(t). \end{aligned} \tag{6}$$

In order to eliminate the time dependence in the distortion D, we proceed to take the time average as follows:

$$\begin{aligned} \bar{D} &= \frac{1}{T_c}\int_0^{T_c} E\{|s(t) - \hat{s}(t)|^2\}\,\mathrm{d}t \\ &= \bar{E}\left\{\left|\sum_{l=N}^{N_*-1} a_l\Phi_l(t)\right|^2\right\} + \bar{E}\left\{\left|\sum_{l=0}^{N-1} (a_l - \hat{a}_l)\Phi_l(t)\right|^2\right\} \\ &\quad + \sum_{l=N}^{N_*-1}\sum_{k=0}^{N-1} E\{a_l^*(a_k - \hat{a}_k)\} \\ &\quad \times \frac{1}{T_c}\underbrace{\int_0^{T_c} \Phi_l^*(t)\Phi_k(t)\,\mathrm{d}t}_{=0} + \sum_{l=N}^{N_*-1}\sum_{k=0}^{N-1} E\{a_l(a_k^* - \hat{a}_k^*)\} \\ &\quad \times \frac{1}{T_c}\underbrace{\int_0^{T_c} \Phi_l(t)\Phi_k^*(t)\,\mathrm{d}t}_{=0} \\ &= \bar{D}_N + \bar{D}_Q \end{aligned} \tag{7}$$

where the bar "$\bar{\ }$" on top of any variable or operator indicates time average, for example $\bar{E}\{\cdot\} = 1/T_c \int_0^{T_c} E\{\cdot\}\,\mathrm{d}t$. Both

terms in the third line of (7) are equal to zero due to the fact that the functions $\Phi_l(t)|_{l=0}^{N_*-1}$ are orthogonal[2] in the interval $0 \le t \le T_c$. Thus, the total distortion introduced by the A/D converter is the sum of the truncation distortion due to the potentially limited number of coefficients N, which is denoted as $\bar{D}_N$, and the quantization distortion due to the finite number of bits used in the quantization of the coefficients $a_l|_{l=0}^{N-1}$, which is denoted as $\bar{D}_Q$.

The first distortion $\bar{D}_N$ introduces truncation error in the reconstruction formula (4), which can be expressed as:

$$e(n) = s(t) - \tilde{s}(t) = s(t) - \sum_{l=0}^{N-1} a_l \Phi_l(t) \tag{8}$$

where the coefficients $a_l|_{l=0}^{N-1}$ are calculated as in (1) in order to minimize the MSE distortion; i.e., to minimize the energy of the error $e(n)$. The distortion $\bar{D}_N$, obtained with N coefficients, can be expressed as

$$\begin{aligned}
\bar{D}_N &= \bar{E}\left\{\left|\sum_{l=N}^{N_*-1} a_l \Phi_l(t)\right|^2\right\} \\
&= \frac{1}{T_c}\int_0^{T_c} E\left\{\left|\sum_{l=N}^{N_*-1} a_l \Phi_l(t)\right|^2\right\} \mathrm{d}t \\
&= \frac{1}{T_c}\int_0^{T_c} E\left\{\sum_{l=N}^{N_*-1}\sum_{m=N}^{N_*-1} a_l a_m^* \Phi_l(t)\Phi_m^*(t)\right\} \mathrm{d}t \\
&= \sum_{l=N}^{N_*-1}\sum_{m=N}^{N_*-1} E\{a_l a_m^*\}\frac{1}{T_c}\int_0^{T_c} \Phi_l(t)\Phi_m^*(t)\,\mathrm{d}t \\
&= \frac{1}{T_c}\sum_{l=N}^{N_*-1} E\{a_l a_l^*\} = \frac{1}{T_c}\left(\sum_{l=0}^{N_*-1}\sigma_l^2 - \sum_{l=0}^{N-1}\sigma_l^2\right) \\
&= \frac{1}{T_c}\left(E_{s,T_c} - \sum_{l=0}^{N-1}\sigma_l^2\right)
\end{aligned} \tag{9}$$

where $E_{s,T_c} = \sum_{l=0}^{N_*-1}\sigma_l^2$ is the energy of the signal in the conversion interval T_c, σ_l^2 is the variance of the coefficient a_l (it is assumed $E\{a_l\} = 0$ for convenience) and the distortion $\bar{D}_N$ is nonnegative by definition. The fourth line in (9) assumes that the functions $\Phi_l(t)|_{l=0}^{N_*-1}$ are orthonormal. When the number of coefficients is N_*, the distortion reaches the zero value and the received signal $s(t)$ can be represented as

$$s(t) = \sum_{l=0}^{N_*-1} a_l \Phi_l(t), \quad 0 \le t \le T_c \tag{10}$$

where the equality holds in the sense that the approximation error has zero energy. From a theoretical point of view, the truncation error $e(n)$ can be made as small as desired; however, in a practical application, this error may be nonzero as the number of coefficients N is limited by system constraints such as complexity and circuitry area. In this case, the coefficients with the largest variance σ_l^2 should be chosen in order to minimize the error energy in (9).

The distortion introduced by the finite number of bits used in the orthogonal-domain quantization of the coefficients, $\bar{D}_Q$, is called quantization error and is commonly measured by the average MSE, given by

$$\bar{D}_Q = \bar{E}\left\{\left|\sum_{l=0}^{N-1}(a_l - \hat{a}_l)\Phi_l(t)\right|^2\right\} = \frac{1}{T_c}\sum_{l=0}^{N-1} D_{Q_l} \tag{11}$$

where the same argument used in (9) is used here to simplify the expression, and $D_{Q_l} = E\{(a_l - \hat{a}_l)^2\}$. A general closed form expression for the individual distortions D_{Q_l} has proven difficult to find except for Gaussian sources; however, for large number of bits b_l, an expression has been found as [27]

$$D_{Q_l}(b_l) = \epsilon_l^2 \sigma_l^2 2^{-2b_l} \tag{12}$$

where ϵ_l^2 is a constant that depends on the probability density function (pdf) of a_l, namely $p_l(a)$, as follows

$$\epsilon_l^2 = \frac{1}{12}\left(\int_{-\infty}^{\infty} \tilde{p}_l(a)^{1/3}\,\mathrm{d}a\right)^3 \tag{13}$$

where $\tilde{p}_l(a) = \sigma_l p_l(\sigma_l a)$. Therefore, the average distortion introduced by the quantization process is

$$\breve{D}_Q = \frac{1}{N}\bar{D}_Q = \frac{1}{NT_c}\sum_{l=0}^{N-1}\epsilon_l^2\sigma_l^2 2^{-2b_l} \tag{14}$$

where the division by N is used to average across the coefficients.

A. Optimum Bit Allocation

At this point, we would like to find the optimal bit allocation among the N coefficients when the desired average number of bits per coefficient at the output of the ADC is a constant B; i.e., we want to find the set of number of bits $b_l|_{l=0}^{N-1}$ constrained to $\sum_{l=0}^{N-1} b_l = BN$ such that the distortion in (14) is minimized. This classical optimization problem can be solved using Lagrange multipliers as shown in Appendix I, leading to

$$b_l = B + \frac{1}{2}\log_2 \frac{\epsilon_l^2\sigma_l^2}{\left(\prod_{l=0}^{N-1}\epsilon_l^2\sigma_l^2\right)^{1/N}}. \tag{15}$$

The optimum solution assigns more bits to the coefficients with larger variance in order to make the distortion of all the coefficients uniform and equal to

$$\breve{D}_{Q*} = \frac{1}{T_c}D_{Q_l} = \frac{1}{T_c}\left(\prod_{l=0}^{N-1}\epsilon_l^2\sigma_l^2\right)^{1/N} 2^{-2B} \le \breve{D}_Q. \tag{16}$$

This bit allocation is equivalent to the concept of *reverse water-filling* found in rate distortion theory [28]. Notice that if the variance of one coefficient is sufficiently small, the resultant

[2]We restrict the ADC distortion analysis presented in Section III to signal projection over orthonormal basis functions for simplicity of the results. However, projection over linearly dependent basis functions can also be employed.

number of bits from (15) could be negative, which in practice would mean that the coefficient should be discarded. Additionally, the optimal solution in (15) can lead to a fractional number of bits b_l, which must be rounded off for practical application. This optimal bit allocation is also well known in the context of video coding, in which the video frame is linearly transformed to another domain before reducing its resolution in order to make more efficient its transmission over a communication channel. This technique is called *block-based transform coding* [29] and assumes that either the original digital data was obtained by means of high-resolution conventional A/D conversion at the Nyquist rate, or did not require any A/D conversion to be generated. This assumption constrains the utilization of the block-based transform coding to discrete applications where high-speed and high-resolution A/D conversion is not required. On the other hand, the technique proposed in this paper is directly intended for A/D conversion since it performs sampling in the same domain where the quantization process is carried out.

B. Comparison Between the Orthogonal Space A/D Conversion and the Conventional Time-Domain A/D Based on Pulse Code Modulation

It is interesting to compare the performance of the A/D conversion based on signal projection with the conventional pulse code modulation (PCM) technique in which each time-domain sample is quantized with a constant number of bits B. The average distortion incurred in PCM, assuming that N samples taken in a T_c window comply with the Nyquist criteria, is [27]

$$\bar{D}_{\mathrm{PCM}} = \frac{1}{T_c}\epsilon_t^2\sigma_t^2 2^{-2B} \tag{17}$$

where the subindex t stands for time, ϵ_t depends on the pdf of a sample of the time domain signal which is assumed stationary, σ_t^2 is the samples' variance, and B is large so that this expression holds in general.

Now, we define a figure of merit of the proposed A/D conversion, the orthogonal space A/D conversion versus time domain PCM A/D conversion gain (G), defined as

$$G = \frac{\bar{D}_{\mathrm{PCM}}}{\breve{D}_Q + \bar{D}_N}. \tag{18}$$

Let G^* be the gain obtained with the optimum number of coefficients N^*

$$G^* = \frac{\bar{D}_{\mathrm{PCM}}}{\breve{D}_{Q*} + \bar{D}_N} \tag{19}$$

which is just the ratio between the distortion of PCM and the distortion introduced by both the limited number of coefficients and the quantization error when carrying out the A/D conversion via signal expansion. Substituting (9), (11), and (17) into (18), we have

$$\begin{aligned} G &= \frac{\epsilon_t^2\sigma_t^2 2^{-2B}}{\frac{1}{N}\sum_{l=0}^{N-1}\epsilon_l^2\sigma_l^2 2^{-2b_l} + E_{s,T_c} - \sum_{l=0}^{N-1}\sigma_l^2} \\ &\le \frac{\epsilon_t^2\sigma_t^2 2^{-2B}}{\left(\prod_{l=0}^{N-1}\epsilon_l^2\sigma_l^2\right)^{1/N} 2^{-2B} + E_{s,T_c} - \sum_{l=0}^{N-1}\sigma_l^2}. \end{aligned} \tag{20}$$

It is interesting to analyze the case in which the number of coefficients reaches the defined value N_*, which makes $\bar{D}_N$ zero. In this case, (20) can be expressed as

$$\begin{aligned} G &= \frac{\epsilon_t^2\sigma_t^2 2^{-2B}}{\frac{1}{N}\sum_{l=0}^{N-1}\epsilon_l^2\sigma_l^2 2^{-2b_l}} \le G^* \\ &= \frac{\epsilon_t^2\sigma_t^2 2^{-2B}}{\left(\prod_{l=0}^{N-1}\epsilon_l^2\sigma_l^2\right)^{1/N} 2^{-2B}} \\ &= \frac{\epsilon_t^2}{\left(\prod_{l=0}^{N-1}\epsilon_l^2\right)^{1/N}} \frac{\frac{1}{N}\sum_{l=0}^{N-1}\sigma_l^2}{\left(\prod_{l=0}^{N-1}\sigma_l^2\right)^{1/N}} \end{aligned} \tag{21}$$

where the last equality follows from the fact that the average energy of the coefficients $a_l|_{l=0}^{N_*-1}$ equals the time samples' variance, since the error in (8) has zero energy. Equation (21) shows the potential gain of the proposed method, as the orthogonal space A/D conversion gain is proportional to the ratio between the arithmetic mean of the orthogonal coefficients variances and the geometric mean of the same variances. Since the arithmetic mean is greater than or equal to the geometric mean, being equal only when all the variances are the same, and in general $\epsilon_t^2 \ge (\prod_{l=0}^{N-1}\epsilon_l^2)^{1/N}$, we have that $G^* \ge 1$ or $\bar{D}_{\mathrm{PCM}} \ge \breve{D}_{Q^*}$, under the same average number of bits B. Notice that a more uneven distribution of the variances leads to a larger gain, which can be advantageous in domains where the variance distribution is known or can be estimated.

C. Reduction in the Number of Basis Coefficients

Assume that instead of being interested in taking advantage of the reduction in distortion offered by the A/D conversion via basis expansion, it is preferred to reduce the number of basis coefficients while keeping a level of distortion that is equal to the one obtained in time-domain A/D conversion with PCM; i.e., $G = 1$. This means that we want to trade distortion gain for reduction in the number of parallel ADCs. The question that arises here is how many coefficients N_{G_u} we need to use such that we obtain a unit gain $(G_u = G = 1)$ for a desired average number of bits B. Since we were unable to symbolically solve for N_{G_u} in terms of B from (20), we instead express B in terms of N_{G_u} as follows:

$$B\left(N_{G_u}\right) = \frac{1}{2}\log_2\left(\frac{\epsilon_t^2\sigma_t^2 - \left(\prod_{l=0}^{N_{G_u}-1}\epsilon_l^2\sigma_l^2\right)^{1/N_{G_u}}}{E_{s,T_c} - \sum_{l=0}^{N_{G_u}-1}\sigma_l^2}\right). \tag{22}$$

This means that if the gain G obtained in (20) is bigger than 1 for some $N \le N_*$, we can reduce the number of coefficients to N_{G_u}, leading to an implementation that requires fewer ADCs than the number of time-interleaved ADCs needed to achieve the same distortion and the same sampling rate. The synchronization challenges that appear in the time-interleaved ADC

architectures due to the very fine time resolution are relaxed in the orthogonal space ADC, because the signal is quantized at the end of the time projection window T_c which will be larger than the Nyquist period. Of course, the distortion gain or the reduction in the number of quantizers come at the cost of the alternative implementation of the circuitry needed in the projection of the input signal over the orthogonal basis.

The results presented so far in this section are suboptimal in the sense that the distortion measure is based on scalar quantization of individual coefficients, and only the bit distribution has been optimized. Better performance can be attained if the distortion measure is optimized jointly over all the coefficients, a concept known as vector quantization. However, practical ADCs are likely to be implemented using only scalar quantization in order to keep low levels of complexity. Optimal bit allocation, together with scalar quantization, provides an interesting gain as shown in (21), with a reasonable compromise in system complexity.

D. Discussion on Optimal Analog to Digital Conversion

At this point we would like to ask a fundamental question regarding the A/D framework presented in this paper: does there exist an orthogonal space that provides the best A/D conversion measured in MSE distortion? In other words, we are asking if we can find a set of orthogonal functions $\Phi_l(t)|_{l=0}^{N_*}$ that expand an input signal $s(t)$ leading to a minimum MSE for a given average number of bits B. Intuitively, the set of orthogonal basis functions should provide the most compact representation, so the number of coefficients N required to achieve some desired level of distortion is minimal. Additionally, from (21) we know that the optimal orthogonal space must minimize the geometric mean of the variances of coefficients. We could try to find the set of optimal orthogonal functions by setting up a constrained optimization problem. However, we instead provide a discussion based on analogy with known results in linear transformations of discrete-time signals. It is well known in linear filter theory that when the Karhunen–Loève transform (KLT) is applied to a zero mean, wide-sense stationary random input vector, the resultant output is a vector of uncorrelated random variables; i.e., the KLT diagonalizes the autocorrelation matrix of the discrete random process [30]. This key observation implies that the KLT provides the most compact representation of the input signal. This result can be easily proven by showing that the geometric mean of the variances of coefficients is minimized when the coefficients are obtained through the KLT [31]. Unfortunately, the KLT is difficult to use in practice as it requires signal stationarity, and the eigenvectors that constitute the basis of the transformation are only available if the statistics of the input signal are known, conditions that are not easily met in real systems. In general, it is desirable for a practical application to have an orthogonal space that is signal independent. To this end, the frequency domain provides a well understood orthogonal space for A/D conversion based on signal projection, which is described in Section IV.

The ADC via signal expansion introduces a time delay as the signal information of the last T_c seconds is transferred to a new domain and condensed into N coefficients. This latency should be properly chosen according to the specific application. For instance, in a communications system, a proper choice of T_c would be a number less than or equal to the transmitted symbol period T. Additionally, the nature of this ADC leads naturally to carrying out digital signal processing (DSP) applications in the same domain used in the A/D conversion itself. The duality between time and some other domains has been extensively studied, and powerful tools are available to carry out the DSP operations. A classical example of this duality is the time-frequency pair, which is studied in Section V in the context of A/D conversion.

IV. An Application: Mixed-Signal Communication Receivers Based on A/D Conversion of Signal Expansions

As an example of an application of the ideas presented here, we will investigate the design of mixed-signal communications receivers. The receivers are mixed-signal in the sense that in their analog front end, signal projection over basis functions is performed before the parallel ADCs are applied. Additionally, the information bits are detected through a discrete matched filter operation that takes place in the domain on which the received signal has been expanded.

A. Transmitted Signal and Channel Model

To elaborate, assume that the signal $s(t)$ is transmitted over a linear communication channel with impulse response $h(t)$

$$r(t) = s(t) * h(t) + z(t), \quad 0 \le t \le T \tag{23}$$

where "$*$" indicates continuous-time convolution and $z(t)$ is additive white Gaussian noise (AWGN). In a typical conventional all-digital linear communication receiver, the received continuous-time signal is first passed through a time-domain A/D converter running at Nyquist rate, and the discrete-time samples are then demodulated by performing a discrete-time linear filtering operation. The following presents a different approach based on the coefficients obtained from A/D conversion after signal expansion.

B. Digital Linear Receivers Based on ADC of Signal Expansion

Assume that the transmitted signal $s(t)$ conveys the information symbol a. In order to obtain an estimate of the transmitted symbol from the set of basis coefficients, we begin by expressing the receiver structure as a linear filtering problem in the time domain

$$\hat{a} = r(t) * p(t)|_{t=T} = \int_0^T r(\tau)p(T-\tau)\,\mathrm{d}\tau \tag{24}$$

where $\hat{a}$ is the symbol estimate, and $p(t)$ is the impulse response of the linear filter demodulator which can be a simple matched filter, a RAKE receiver, an MMSE receiver, etc. The output of this filter is sampled at $t = T$. For convenience, (24) is expressed as

$$\hat{a} = \int_0^T r(\tau)p(T-\tau)\,\mathrm{d}\tau = \int_0^T r(\tau)g^*(\tau)\,\mathrm{d}\tau \tag{25}$$

where we define $g^*(\tau) = p(T-\tau)$. Now, we proceed to segment the symbol duration time T into M time-slots of duration T_c. We define the following signals

$$r_m(t) = r(t)w_m(t) \tag{26}$$

$$g_m(t) = g(t)w_m(t) \tag{27}$$

for $m = 0, \ldots, M-1$, and the window $w_m(t)$ introduced in (27) has been selected as rectangular for simplicity of the analysis although, as mentioned earlier, other windows with desired characteristics could be used instead.

Using these definitions, the linear receiver output in (24) can be expressed as

$$\begin{aligned}\hat{a} &= \sum_{m=0}^{M-1} \int_{mT_c}^{(m+1)T_c} r(\tau)g^*(\tau)\,\mathrm{d}\tau \\ &= \sum_{m=0}^{M-1} \int_{mT_c}^{(m+1)T_c} r_m(\tau)g_m^*(\tau)\,\mathrm{d}\tau \\ &= \sum_{m=0}^{M-1} \int_{-\infty}^{\infty} r_m(\tau)g_m^*(\tau)\,\mathrm{d}\tau \end{aligned} \tag{28}$$

in which the integral in (24) has been segmented into M integrals that run over intervals of duration T_c each, such that $T = MT_c$.

In order to express the matched filter operations in the new conversion domain, the signal expansion over the basis functions $\Phi_l(t)$ is used to represent both the segmented received signal and segmented receive filter, leading to

$$\begin{aligned}\hat{a} &= \sum_{m=0}^{M-1} \int_{-\infty}^{\infty} r_m(\tau)g_m^*(\tau)\,\mathrm{d}\tau \\ &= \sum_{m=0}^{M-1} \int_{-\infty}^{\infty} \sum_{n=0}^{\infty} R_m(n)\Phi_n(\tau) \sum_{l=0}^{\infty} G_m^*(l)\Phi_l^*(\tau)\,\mathrm{d}\tau \\ &= \sum_{m=0}^{M-1} \sum_{n=0}^{\infty}\sum_{l=0}^{\infty} R_m(n)G_m^*(l) \int_{-\infty}^{\infty} \Phi_n(\tau)\Phi_l^*(\tau)\,\mathrm{d}\tau \\ &= \sum_{m=0}^{M-1} \sum_{n=0}^{\infty}\sum_{l=0}^{\infty} R_m(n)G_m^*(l)\psi_{n,l} \\ &\approx \sum_{m=0}^{M-1} \sum_{n=0}^{N-1}\sum_{l=0}^{N-1} R_m(n)G_m^*(l)\psi_{n,l} \end{aligned} \tag{29}$$

where $R_m(n)|_{n=0}^{N-1}$ and $G_m(l)|_{l=0}^{N-1}$ are the best MSE coefficients representation as explained in (4), which requires reversing the linear transformation of (3). Note that the series expansion in (29) has been truncated, leading to some degree of error. Althuogh this truncation error should in principle degrade the receiver performance, we will show in the following examples that any desired performance can be achieved if the tradeoff between complexity in terms of number of coefficients N, and sampling speed $\Delta F_c = 1/T_c = M/T$, is adequately set up. Note that if the basis functions are orthonormal, (29) reduces

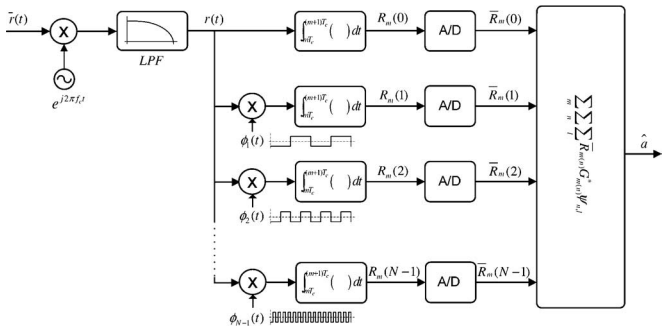

Fig. 2. Mixed-signal receiver block diagram with ADC via signal expansion. Binary basis functions are shown as an example.

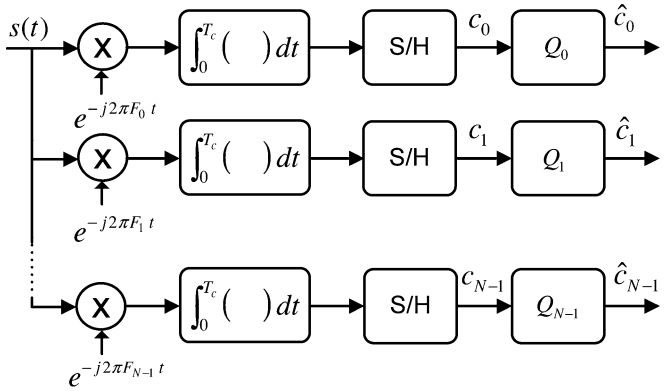

Fig. 3. Block diagram of the frequency domain A/D converter.

to

$$\hat{a} \approx \sum_{m=0}^{M-1} \sum_{n=0}^{N-1} R_m(n)G_m^*(n) \tag{30}$$

which reduces the complexity of detection. The tradeoff between the choice of the basis functions, complexity of the detection formula, and the degree of truncation error is fundamental in the receiver design. Fig. 2 illustrates the mixed-signal receiver architecture.

V. Analog to Digital Conversion in the Frequency Domain

The frequency domain emerges as an appealing domain for the analog to digital conversion of signals with very large bandwidth, since, in principle, it relaxes the extremely fine time resolution needed in time-domain ADCs and provides a scalable architecture. The timing requirements are relaxed since the sampling is performed at a rate that is lower than the one imposed by Nyquist criteria. Fig. 3 shows the block diagram of the frequency domain ADC in which the complex exponential functions that constitute the orthogonal basis allow sampling of the continuous-time signal at the frequencies $F_l|_{l=0}^{N-1}$, leading to the set of frequency coefficients

$$c_l = \int_0^{T_c} s(t)e^{-j2\pi F_l t}\,\mathrm{d}t, \quad l = 0, \ldots, N-1. \tag{31}$$

These coefficients are then quantized by a set of quantizers $Q_l|_{l=0}^{N-1}$ which, in turn, produce the ADC output digital coefficients $\hat{c}_l|_{l=0}^{N-1}$. The frequency sample spacing $\Delta F = F_l - F_{l-1}$ complies with $\Delta F \leq (1)/(T_c)$ in order to avoid aliasing in the discrete-time domain [32]. Thus, the optimal number of coefficients N_* necessary to fully sample the signal spectrum with bandwidth W, without introducing time aliasing, is proportional to the time-bandwidth product[3]

$$N_* = \left\lceil \frac{W}{\Delta F} + 1 \right\rceil \geq \lceil WT_c + 1 \rceil \tag{32}$$

where the operator $\lceil\ \rceil$ is used to ensure that N_* is the closest upper integer that avoids discrete-time aliasing. When $\Delta F = (1)/(T_c)$, (32) becomes an equality and the discrete-time alias-free condition is satisfied without oversampling of the frequency spectrum.

Note that the frequency-domain ADC is fundamentally different from the ADC architectures based on filter bank theory [14], [16]. This simple but fundamental difference lies in the fact that the frequency domain ADC samples the expansion of time-segments of the received signal, whereas the filter bank approach performs frequency channelization. The computation of the Fourier samples, via mixing and integration, can be thought of as synthesizing a filter bank. However, these filters are very broad with smooth transitions. In fact, the frequency response of the branches in Fig. 3 overlap with each other, but this overlapping does not introduce ADC distortion. On the other hand, the filter bank approach requires filters with very sharp roll-off and any leakage between the channels will seriously degrade the ADC performance. This is an important motivation for the implementation of the frequency domain ADC.

A. Example

Let us consider a stationary zero-mean Gaussian continuous source with variance σ_t^2, bandwidth $W = 2$ GHz @-55 dB, central frequency $F_c = 7$ GHz and a power spectrum density (PSD) shown in Fig. 4(a). Notice that in this case the signal PSD provides the information about the coefficient's variance distribution needed in the optimal bit allocation. The signal is segmented in intervals of $T_c = 3$ ns to be A/D converted, thus requiring a frequency spacing between samples of $\Delta F = 1/T_c = 333.33$ MHz to avoid aliasing in the discrete-time equivalent signal. The bits are optimally distributed among the coefficients as indicated by (15), leading to the set of curves of MSE distortion vs. average number of bits B plotted in Fig. 4(b). The MSE distortion for PCM is also shown for comparison purposes. The A/D conversion gain (G) is plotted in Fig. 4(c) against the number of coefficients N $(N_* = 7)$ for several values of average number of bits B. These figures show the potential gain of performing the A/D conversion in the frequency domain together with optimal bit allocation, especially when the target average number of bits is low. For this example, a gain of up to 3.35 (5.25 dB) can be achieved when $N_* = 7$ coefficients are implemented.

Furthermore, assume that a mono-bit (i.e., $B = 1$) implementation is desired and lowering the sampling rate is the main concern in the design. So, we would like to trade distortion gain for a lower sampling rate of the ADCs. Fig. 4(c) shows that a mono-bit implementation with $N = 5$ coefficients (9 real-valued ADCs, since the DC-frequency coefficient requires just one ADC while the other complex-valued frequency samples require two ADCs) achieves the same distortion rate of a time-domain ADC with PCM. However, the frequency-domain ADC operates at $1/T_c = 333.33$ MHz whereas the time-domain ADC requires a sampling rate of 4 GHz to meet the Nyquist criterion. If a time-interleaved architecture is implemented in the time domain ADC to reduce the speed of the comparators to 333.33 MHz, a total of 12 ADCs would have to be used, leading to an implementation that requires three more ADCs than the frequency domain ADC implementation. Notice that although the MSE distortion in (12) is in general only valid for a large number of bits; for Gaussian sources, the expression holds asymptotically even for a small number of bits [28], so the curves in Fig. 4 are exact under the assumptions of this example.

VI. Signal to Noise and Distortion Ratio (SNDR) of the Frequency-Domain ADC

In this Section we calculate the signal to noise and distortion error for the frequency domain ADC that includes gain distortions, timing errors, frequency offsets, and additive noise in all the paths of the ADC. It is assumed that a testing sinusoidal signal $r(t) = A\cos(2\pi F_x t)$ is driven to the ADC input. The frequency samples provided by the ADC under distortion and noise can be expressed as

$$\tilde{R}(F_n) = g_n \int_{-Tc/2}^{T_c/2} r(t - \Delta t_n) e^{-j2\pi(F_n - \Delta F n)t}\, \mathrm{d}t + o_n \qquad n = 0, \ldots, N-1 \tag{33}$$

where g_n is the gain distortion, Δt_n is the time error, ΔF_n is the frequency offset, and o_n is the additive noise associated with the nth frequency sample. For the specific case of a test signal $r(t) = A\cos(2\pi F_x t)$ and using the identity $\cos(2\pi F_x(t - \Delta t_n)) = \cos(2\pi F_x t)\cos(2\pi F_x \Delta t_n) + \sin(2\pi F_x t)\sin(2\pi F_x \Delta t_n)$, (33) reduces to

$$\begin{aligned}\tilde{R}(F_n) &= g_n \int_{-T_c/2}^{T_c/2} A\cos(2\pi F_x(t - \Delta t_n)) \\ &\quad \times e^{-j2\pi(F_n - \Delta F n)t}\, \mathrm{d}t + o_n \\ &= A g_n \Bigg(\cos(2\pi F_x \Delta t n) \\ &\quad \times \int_{-T_c/2}^{T_c/2} \cos(2\pi F_x t) e^{-j2\pi(F_n - \Delta F n)t}\, \mathrm{d}t\end{aligned}$$

[3]Because signals found in applications are time-limited, the term bandwidth here refers to the range of frequencies in which the signal power is larger than some defined power level; for instance, many signal bandwidths are defined at 3 dB of attenuation, although more conservative attenuation could be desirable for some applications such as A/D conversion. Moreover, the bandwidth W in this paper is the bandwidth of the time-segmented signal which, in general, is larger than the bandwidth of the signal $s(t)$, as the segmentation introduces sidelobes that should be sampled in order to obtain lower distortion error.

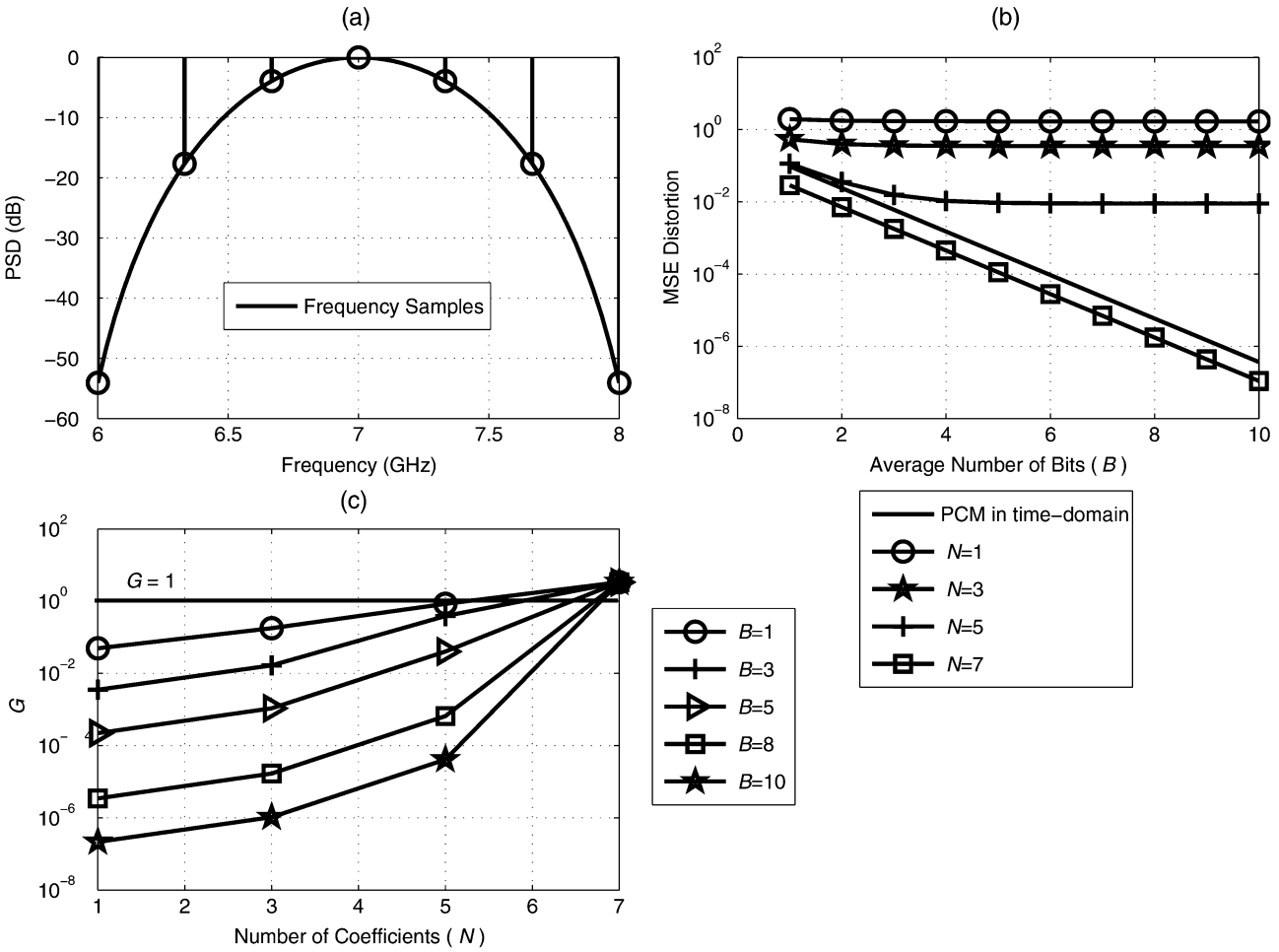

Fig. 4. (a) Raised cosine shaped power spectrum of the Gaussian source to be A/D converted. (b) Comparison between the MSE distortion of the time-domain PCM ADC with the MSE distortion of the ADC in frequency domain with optimal bit allocation. (c) The A/D conversion gain (G) versus the number of coefficients (N) for different average number of bits.

$$
\begin{aligned}
&+ \sin(2\pi F_x \Delta t n) \\
&\times \int_{-T_c/2}^{T_c/2} \sin(2\pi F_x t) e^{-j2\pi(F_n - \Delta F n)t}\, \mathrm{d}t \Bigg) \\
&= A g_n \Bigg(\cos(2\pi F_x \Delta t n) \\
&\times \int_{-T_c/2}^{T_c/2} \cos(2\pi F_x t) e^{-j2\pi(F_n - \Delta F n)t}\, \mathrm{d}t \\
&- j \sin(2\pi F_x \Delta t n) \\
&\times \int_{-T_c/2}^{T_c/2} \cos(2\pi F_x t) e^{-j2\pi(F_n - \Delta F n)t}\, \mathrm{d}t \Bigg) \\
&= A g_n R(F_n + \Delta F_n) e^{-j2\pi F_x \Delta t_n} + o_n \qquad (34)
\end{aligned}
$$

where $R(F_n)$ is given by

$$
R(F_n) = \frac{\sin(\pi T_c (F_n - F_x))}{\pi T_c (F_n - F_x)}. \qquad (35)
$$

It can be noted from (35) that if there are no frequency offsets, only the sample $R(F_x)$ will be nonzero since all the other samples align with the nulls of (35).

The SNDR will be given by the ratio of the power at the frequency of interest F_x, and the sum of the powers at all the other frequencies F_n. Note that the phase rotation of the sample $\tilde{R}(F_x)$ due to time jitter will degrade the SNDR. To see this, let us express $\tilde{R}(F_x)$ in real and imaginary parts

$$
\begin{aligned}
\tilde{R}(F_x) = {} & A g_x R(F_n + \Delta F_x) \cos(2\pi F_x \Delta t_x) \\
& + o_{xR} + j * (A g_x R(F_n + \Delta F_x) \\
& \times \sin(2\pi F_x \Delta t_x) + o_{xI}) \qquad (36)
\end{aligned}
$$

where $o_{xR} = \mathrm{Re}\{o_x\}$ and $o_{xI} = \mathrm{Im}\{o_x\}$. The real part of $\tilde{R}(F_x)$ corresponds to the signal component whereas the imaginary part of $\tilde{R}(F_x)$ introduces distortion, where the amount of jitter Δt_x determines how much distortion is introduced. Thus,

the SNDR is given by

$$\text{SNDR} = 10\log_{10}\left(\frac{\mathrm{E}\{|\mathrm{Re}\{\tilde{R}(F_x)\}|^2\}}{\sum_{\substack{n=0\\n\neq x}}^{N-1}\mathrm{E}\{|\tilde{R}(F_n)|^2\}+\mathrm{E}\{|\mathrm{Im}\{\tilde{R}(F_x)\}|^2\}}\right) \tag{37}$$

where the orthogonality among the frequency samples allows to express the expected value of the sum as a sum of expected values. The numerator in (37) is the signal power component which, as shown in Appendix II, can be approximated as

$$\mathrm{E}\{|\mathrm{Re}\{\tilde{R}(F_x)\}|^2\} \approx A^2\sigma_g^2\left(1-\frac{\pi^2}{3}\sigma_{\Delta F}^2\right) \times\left(1-4\pi^2\sigma_{\Delta tx}^2\right)+\frac{1}{2}\sigma_o^2 \tag{38}$$

where $\sigma_g^2 = E\{g_n^2\}|_{n=0}^{N-1}, \sigma_{\Delta F}^2 = (E\{\Delta F_n^2\})/(\Delta F_c^2)|_{n=0}^{N-1}$, and $\sigma_{\Delta tx}^2 = F_x^2 E\{\Delta t_x^2\}$, which assumes that the distortions in all the paths have the same second order moments. Notice that the parameters $\sigma_{\Delta F}^2$ and $\sigma_{\Delta tx}^2$ have included the normalization factors $(1)/(\Delta F_c^2)$ and F_x^2, respectively.

The noise terms in the sum of the denominator of (37) are shown in Appendix II to be

$$\mathrm{E}\{|\tilde{R}(F_n)|^2\} \approx A^2\sigma_{\Delta F}^2\sigma_g^2(n-x)^{-2}+\sigma_o^2. \tag{39}$$

The noise term due to the imaginary part of $\tilde{R}(F_x)$ is also approximated in Appendix II as

$$\mathrm{E}\{|\mathrm{Im}\{\tilde{R}(F_x)\}|^2\} \approx A^2\sigma_g^2(1-\frac{\pi^2}{3}\sigma_{\Delta F}^2) \times\left(4\pi^2\sigma_{\Delta tx}^2\right)+\frac{1}{2}\sigma_o^2. \tag{40}$$

These results lead to (41) for the SNDR (see bottom of the page). This expression reveals several interesting results. For instance, the gain variance has no effect on the SNDR if the additive noise second order moment is zero, which in practice means little impact on the SNDR for reasonable values of σ_o^2.

Setting $\sigma_g^2 = 0, \sigma_{\Delta tx}^2 = 0$, and $\sigma_o^2 = 0$, we obtain the SNDR due to frequency offset

$$\text{SNDR} = 10\log_{10}\left(\frac{(1-\frac{\pi^2}{3}\sigma_{\Delta F}^2)}{\sigma_{\Delta F}^2\sum_{\substack{n=0\\n\neq x}}^{N-1}(n-x)^{-2}}\right). \tag{42}$$

With $\sigma_g^2 = 0, \sigma_{\Delta F}^2 = 0$, and $\sigma_o^2 = 0$, we find the SNDR due to time jitter

$$\text{SNDR} = 10\log_{10}\left(\frac{(1-4\pi^2\sigma_{\Delta tx}^2)}{4\pi^2\sigma_{\Delta tx}^2}\right) \tag{43}$$

and setting $\sigma_g^2 = 0, \sigma_{\Delta F}^2 = 0$, and $\sigma_{\Delta t_x}^2 = 0$, we find the SNDR due to amplitude offset

$$\text{SNDR} = 10\log_{10}\left(\frac{\frac{1}{2}}{(N-\frac{1}{2})}\right). \tag{44}$$

Fig. 5 illustrates the impact of the implementation impairments on the SNDR. Each plot shows the impact of two impairments on the SNDR; the left column shows the 3-D plots and the right column shows the corresponding isolines. The number of frequency samples is $N = 5$.

A. Example

To understand the implication of the results presented in Fig. 5, let us consider a practical SNDR test scenario. Assume that a $F_x = 5$ GHz tone drives the frequency ADC. The sampling period T_c is chosen to be five periods of the sinusoidal signal, $T_c = 1$ ns, which leads to a frequency spacing between samples of $\Delta F_c = 1$ GHz. Additionally, the ADC has $N = 5$ branches which implies that 5 samples of the spectrum are taken for each T_c sec window. Thus, the 5 samples are uniformly distributed around the tone frequency leading to the frequency range [3,7] GHz. If the frequency samples do not suffer from frequency offset, only the sample at $F_x = 5$ will be nonzero as the other samples will lie at the nulls of the spectrum of the input signal. However, frequency offset will result in all the components collecting some undesired energy, degrading the SNDR as defined in (37). To obtain a sense of practical levels of frequency offset and timing errors that can be tolerated in this specific example, let us assume that from Fig. 5 we conclude that acceptable SNDR value is around 40 dB. This is achieved with a normalized frequency offset second moment $\sigma_{\Delta F}^2$ near 10^{-6} GHz^2, together with a normalized time error with second moment around $10^{-6}\,\mathrm{s}^2$. Then, the second order moment of the frequency offset will be equal to $E\{\Delta F_n^2\} = \Delta F_c^2\sigma_{\Delta F}^2 = 10^{18}10^{-6} = 10^{12}\,\mathrm{GHz}^2$. Now, assuming a deterministic frequency offset, a second order moment of $10^{12}\,\mathrm{GHz}^2$ is achieved by a fixed offset of 1 MHz or less. So, for the highest oscillator frequency, i.e., the one at 10 GHz, a requirement of only 10^3 parts per million (ppm) is needed. In the case of timing errors, the target SNDR is achieved with normalized second moment of around 10^{-6}, which leads to an absolute time error second moment of $E\{\Delta t_n^2\} = (\sigma_{\Delta t_n}^2)/(F_x^2) = (10^{-6})/(25*10^{18}) = 4*10^{-26}\,\mathrm{s}^2$. Once again, assuming a fixed time offset, a second order moment of $4*10^{-26}\mathrm{s}$ is achieved with a time offset of 0.2 ps. Thus, up to 0.2 ps of time offset are allowed in time windows of 1 ns for the specific example considered here. Lastly, an acceptable value of AWGN noise is around 10^{-6} W/Hz.

$$\text{SNDR} = 10\log_{10}\left(\frac{A^2\sigma_g^2(1-\frac{\pi^2}{3}\sigma_{\Delta F}^2)(1-4\pi^2\sigma_{\Delta tx}^2)+\frac{1}{2}\sigma_o^2}{A^2\sigma_g^2\left(\sigma_{\Delta F}^2\sum_{\substack{n=0\\n\neq x}}^{N-1}(n-x)^{-2}+(1-\frac{\pi^2}{3}\sigma_{\Delta F}^2)(4\pi^2\sigma_{\Delta tx}^2)\right)+(N-\frac{1}{2})\sigma_o^2}\right). \tag{41}$$

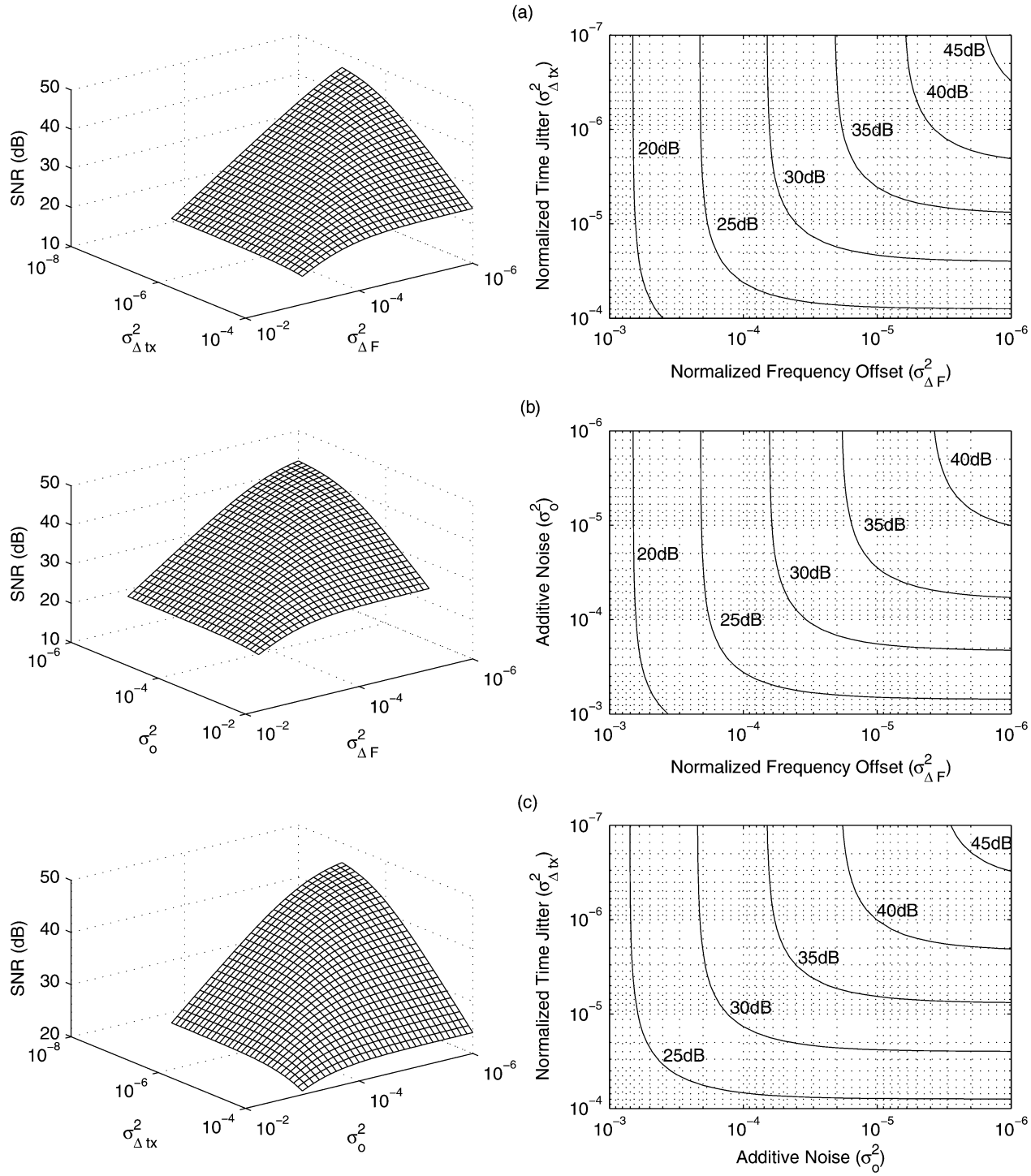

Fig. 5. Signal to noise and distortion ratio for frequency domain ADC with $N = 5$. No gain distortion is included (i.e., $E\{g_n^2\} = 1$). (a-left column) Normalized timing errors second moment ($\sigma^2_{\Delta t_x}$) versus normalized frequency offset second moment ($\sigma^2_{\Delta F}$) for $\sigma^2_o = 10^{-6}$, and in (a-right column) isolines. (b-left column) Additive noise second moment (σ^2_o) versus normalized frequency offset second moment ($\sigma^2_{\Delta F}$) for $\sigma^2_{\Delta t_x} = 10^{-6}$, and in (a-right column) isolines. (c-left column) Normalized timing errors second moment ($\sigma^2_{\Delta t_x}$) versus additive noise second moment (σ^2_o) for $\sigma^2_{\Delta F} = 10^{-6}$, and in (c-right column) isolines.

VII. Frequency-Domain Mixed-Signal Receivers

The frequency domain ADC architecture allows the implementation of linear and nonlinear receivers with lower sampling rates and lower bit resolution requirements [33].

A. Mixed-Signal Multicarrier Receiver

In this example, we consider the design of a mixed-signal multicarrier receiver, summarized in the detection formula of (29). In order to provide a practical example, we use the system

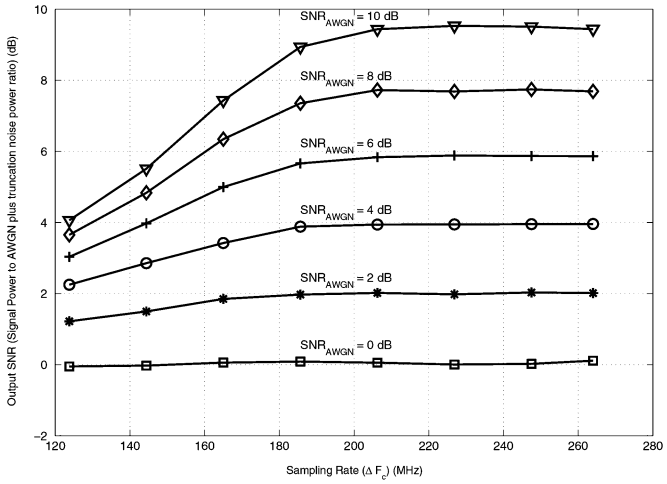

Fig. 6. Output SNR of the mixed-signal multicarrier receiver implemented with $N = 3$ coefficients, versus the sampling rate for different values of $\mathrm{SNR}_{\mathrm{AWGN}} = 10 * \log_{10}(E_b/N_o)$.

specifications of the multiband UWB OFDM receiver presented in the standard draft IEEE P802.15-03/268r1 [34]. The multicarrier signal is composed of 128 tones, with a frequency spacing of 4.125 MHz and a central frequency that lies in any of the UWB subbands. The receiver proposed in [34] requires two conventional time domain ADC (for I/Q paths) operating at a Nyquist rate of 528 Ms/s. Additionally, up to seven times this speed will be required to fully exploit all the UWB spectrum.

For our receiver design we consider a single 528 MHz subband. As illustrated in Fig. 2, the received signal is downconverted to baseband frequencies, and then is projected onto the set of basis functions. We use the complex exponential functions as the basis functions, with $N = 3$ frequency samples. Fig. 6 shows the signal to noise ratio (SNR) at the output of the discrete frequency matched filter (AWGN noise power plus truncation error power) versus the sampling rate ΔF_c, for different values of $\mathrm{SNR}_{\mathrm{AWGN}} = 10 * \log_{10}(E_b/N_o)$, where E_b is the signal energy and $N_o/2$ is the two-sided power spectral density of the AWGN noise. The figure shows the required sampling rate to make negligible the truncation error compared with AWGN noise. For practical values of SNR, the truncation error is indeed negligible. For example, in a UWB multiband multicarrier application, the $\mathrm{SNR}_{\mathrm{AWGN}}$ ranges between 4.0 dB and 4.9 dB or even lower if coding is taken into account, which makes this receiver an interesting possibility to lower the sampling rate requirements, especially as more subbands are included in the design. However, for applications operating at larger $\mathrm{SNR}_{\mathrm{AWGN}}$ values, the truncation error could become the dominant impairment and needs to be taken into consideration.

VIII. Conclusion

We have explored analog to digital conversion of signal expansions, where instead of sampling the signal in the time domain as it has been conventionally done in A/D conversion, the input analog signal is projected over a set of basis functions before quantization takes place. Quantization is then carried out over the coefficients obtained from this projection. This A/D conversion technique provides a potential gain over time-domain ADCs when optimal bit allocation is used in the quantization process of the coefficients. Additionally, a reduction of the sampling rate is achieved as the A/D conversion is performed at the end of a properly chosen time window of T_c seconds during which the signal is projected. The sampling rate reduction comes at the cost of increasing the number of basis functions on which the continuous-time signal is projected, leading to a fundamental tradeoff between complexity and sampling rate. Furthermore, the new technique possesses some degree of flexibility in the design as trading between speed and distortion can be achieved by properly choosing the conversion time T_c and the number of coefficients N.

We have also established a framework for a family of mixed-signal communications receivers as a potential application of the ADC framework presented here, and closed form expressions for symbol detection have been found. The new receiver architecture provides a means to implement wide-band communication receivers with parallel processing at lower sampling speeds, without time domain signal reconstruction.

As a specific application, the frequency domain constitutes an appealing domain to perform the A/D conversion of ultra-wideband signals. Moreover, having samples of the signal spectrum encourages implementing many communications and signal processing applications in the frequency domain. Specifically, it was shown how the matched filter can be easily implemented, even though segmentation of the time-domain signal is used to reduce the number of coefficients. Additional robustness is obtained by the ADC in the frequency domain as it naturally filters narrow-band interference that lies away from the spectrum points where samples are taken. As an example in communication systems using multicarrier transmission, the proposed A/D conversion in the frequency domain goes together with a very simple frequency domain implementation of the digital correlators needed for the estimation of the information symbols. Although the frequency domain is perhaps the oldest and best understood domain besides the time-domain, other domains may have desirable characteristics when carrying out A/D conversion. For example, from a circuit implementation point of view, generation of the sinusoidal signals operating at frequencies $F_l|_{l=0}^{N-1}$ used for the projection of the input signal in the frequency domain ADC might lead to higher levels of complexity and power consumption. Lower complexity can be achieved by generating binary waveforms instead of sinusoidal ones. Transformations that use orthogonal signals with binary waveforms include the Hadamard transform [35], [36], Walsh [35]–[37] and Walsh–Fourier [38] transform, and the Haar wavelet transform [39].

All digital systems that interface with real-world signals, such as voice, audio, communication waveforms, array processing etc, can be implemented with the A/D conversion ideas presented in this paper. The solution provided is especially beneficial for ultra-wideband systems, such as communications and geolocation.

APPENDIX I

Given a desired average number of bits B, we want to allocate a total number of bits NB among the N coefficients, so that the error in (14) is minimized. The Lagrange multiplier method provides a solution to this constrained optimization problem as

$$J(b_l|_{l=0}^{N-1}) = \sum_{l=0}^{N-1} \epsilon_l^2 \sigma_l^2 2^{-2b_l} + \lambda \left(\sum_{l=0}^{N-1} b_l - BN \right) \quad (45)$$

where λ must be chosen to satisfy

$$\sum_{l=0}^{N-1} b_l = BN. \quad (46)$$

Now, setting to zero the derivative of (45) with respect to b_l leads to

$$\frac{\partial J}{\partial b_l} = -(2\ln 2)\epsilon_l^2 \sigma_l^2 2^{-2b_l} = -\lambda. \quad (47)$$

λ is determined by the taking the product of (47) for all l, leading to

$$\lambda^N = (2\ln 2)^N \left(\prod_{l=0}^{N-1} \epsilon_l^2 \sigma_l^2 \right) 2^{-2\sum_l b_l}$$

$$= (2\ln 2)^N \left(\prod_{l=0}^{N-1} \epsilon_l^2 \sigma_l^2 \right) 2^{-2NB} \quad (48)$$

so that

$$\lambda = (2\ln 2) \left(\prod_{l=0}^{N-1} \epsilon_l^2 \sigma_l^2 \right)^{1/N} 2^{-2B}. \quad (49)$$

After substitution in (47), the optimum bit allocation is found to be

$$b_l = B + \frac{1}{2} \log_2 \frac{\epsilon_l^2 \sigma_l^2}{\left(\prod_{l=0}^{N-1} \epsilon_l^2 \sigma_l^2 \right)^{1/N}}. \quad (50)$$

APPENDIX II

For simplicity of the analysis, we assume that the impairments $\Delta F_n, \Delta t_n$, and o_n have equal variance in all the paths, i.e., $\sigma_g^2 = E\{g_n^2\}|_{n=0}^{N-1}, \sigma_{\Delta F}^2 = (E\{\Delta F_n^2\})/(\Delta F_c^2)|_{n=0}^{N-1}, \sigma_{\Delta t_n}^2 = F_x^2 E\{\Delta t_n^2\}|_{n=0}^{N-1}$, and $\sigma_o^2 = E\{o_n^2\}|_{n=0}^{N-1}$. Note also that the parameters $\sigma_{\Delta F}^2$ and $\sigma_{\Delta t_n}^2$ are normalized with the factors $(1)/\Delta F_c^2$ and F_x^2, respectively.

The SNDR is given by

$$\text{SNDR} = 10 \log_{10} \left(\frac{\mathrm{E}\{|\mathrm{Re}\{\tilde{R}(F_x)\}|^2\}}{\sum_{\substack{n=0 \\ n \neq x}}^{N-1} \mathrm{E}\{|\tilde{R}(F_n)|^2\} + \mathrm{E}\{|\mathrm{Im}\{\tilde{R}(F_x)\}|^2\}} \right). \quad (51)$$

The exact calculation of the expected values involved in (51) is difficult. A simpler and perhaps more meaningful solution is provided by using truncated Taylor expansions. The following Taylor expansions will be used:

$$\left(\frac{\sin(x)}{x} \right)^2 \approx 1 - \frac{x^2}{3} \quad \text{expansion around } x = 0 \quad (52)$$

$$\cos^2(x) \approx 1 - x^2 \quad \text{expansion around } x = 0 \quad (53)$$

$$\sin^2(x) \approx x^2 \quad \text{expansion around } x = 0. \quad (54)$$

The signal power term is given by

$$\mathrm{E}\{|\mathrm{Re}\{\tilde{R}(F_x)\}|^2\}$$

$$= \mathrm{E}\left\{ A^2 g_x^2 \left(\frac{\sin(\pi T_c(\Delta F_x))}{\pi T_c(\Delta F_x)} \right)^2 \cos^2(2\pi F_x \Delta t_x) + o_{xR}^2 \right\}$$

$$\approx A^2 \sigma_g^2 (1 - \frac{\pi^2}{3}\sigma_{\Delta F}^2)(1 - 4\pi^2 \sigma_{\Delta t_x}^2) + \frac{1}{2}\sigma_o^2. \quad (55)$$

The noise terms in the sum of the denominator of (51) are approximated as

$$\mathrm{E}\{|\tilde{R}(F_n)|^2\}$$

$$= \mathrm{E}\{A^2 g_n^2 \left(\frac{\sin(\pi T_c(F_n + \Delta F_n - F_x))}{\pi T_c(F_n + \Delta F_n - F_x)} \right)^2 + o_n^2\}$$

$$\approx A^2 \sigma_{\Delta F}^2 \sigma_g^2 (n - x)^{-2} + \sigma_o^2, \quad n \neq x. \quad (56)$$

The noise term due to the imaginary part of $\tilde{R}(F_x)$ is approximated as

$$\mathrm{E}\{|\mathrm{Im}\{\tilde{R}(F_x)\}|^2\}$$

$$= \mathrm{E}\left\{ A^2 g_x^2 \left(\frac{\sin(\pi T_c(\Delta F_x))}{\pi T_c(\Delta F_x)} \right)^2 \sin^2(2\pi F_x \Delta t_x) + o_{xI}^2 \right\}$$

$$\approx A^2 \sigma_g^2 \left(1 - \frac{\pi^2}{3}\sigma_{\Delta F}^2 \right) \left(4\pi^2 \sigma_{\Delta tx}^2 \right) + \frac{1}{2}\sigma_o^2. \quad (57)$$

These results lead to (58) for the SNDR (see the bottom of the page).

REFERENCES

[1] R. H. Walden, "Analog-to-digital converter survey and analysis," *IEEE J. Sel. Areas Commun.*, vol. 17, pp. 539–550, Apr. 1999.

[2] J. van Valverg and R. J. van de Plassche, "An 8-bit 650 MHz folding ADC," *IEEE J. Solid State Circuits*, vol. 27, pp. 1662–1666, Dec. 1992.

[3] K. Poulton, K. L. Knudsen, J. J. Corcoran, K. C. Wang, R. B. Nubling, R. L. Pierson, M.-C. F. Chang, P. M. Asbeck, and R. T. Huang, "A 6-b, 4GSals GaAs HBT ADC," *IEEE J. Solid-State Circuits*, vol. 30, no. 10, pp. 1109–1118, Oct. 1995.

[4] K. Nary, R. Nubling, S. Beccue, W. Colleran, J. Penney, and K. Wang, "An 8-bit, 2-gigasample per second analog to digital converter," in *GaAs IC Symp. Tech. Dig.*, vol. 17, Oct. 1995, pp. 246–303.

[5] K. Sone, N. Naotoshi, Y. Nishida, M. Ishida, Y. Sekine, and M. Yotsuyanagi, "A 10b 100 Ms/s pipelined subranging BiCMOS ADC," *IEEE*

$$\text{SNDR} = 10 \log_{10} \left(\frac{A^2 \sigma_g^2 (1 - \frac{\pi^2}{3}\sigma_{\Delta F}^2)(1 - 4\pi^2 \sigma_{\Delta tx}^2) + \frac{1}{2}\sigma_o^2}{A^2 \sigma_g^2 \left(\sigma_{\Delta F}^2 \sum_{\substack{n=0 \\ n \neq x}}^{N-1} (n - x)^{-2} + (1 - \frac{\pi^2}{3}\sigma_{\Delta F}^2)(4\pi^2 \sigma_{\Delta tx}^2) \right) + (N - \frac{1}{2})\sigma_o^2} \right). \quad (58)$$

International Solid-State Circuits Conf., ISSEC'93 Dig. Tech. Papers, vol. 36, pp. 66–67, Feb. 1993.
[6] W. T. Colleran, T. H. Phan, and A. A. Abidi, "A 10b 100 Ms/s pipelined A/D converter," *GaAs IC Symp. Tech. Dig.*, vol. 36, pp. 68–69, Feb. 1993.
[7] C. Schiller and P. Byrne, "A 4-GHz 8-b ADC system," *IEEE J. Solid State Circuits*, vol. 26, pp. 1781–1789, Dec. 1991.
[8] R. M. Gray, "Oversampled sigma-delta modulation," *IEEE Trans. Commun.*, vol. COM-35, pp. 481–489, May 1987.
[9] P. Aziz, H. Sorensen, and J. Van der Spiegel, "Multiband sigma-delta modulation," *Electron. Lett.*, vol. 29, no. 9, pp. 760–762, Apr. 1993.
[10] I. Galton and H. T. Jensen, "Delta-sigma modulator based A/D conversion without oversampling," *IEEE Trans. Circuits Syst. II:Analog Digit. Signal Process.*, vol. 42, no. 12, pp. 773–784, Dec. 1995.
[11] I. D. O'Donnell, M. S. W. Chen, S. B. T. Wang, and R. W. Brodersen, "An integrated, low power, ultra-wideband transceiver architecture for low-rate, indoor wireless systems," *IEEE CAS Workshop Wireless Communications and Networking*, Pasadena, CA, Sep. 2002.
[12] S. Hoyos, B. M. Sadler, and G. R. Arce, "Dithering and sigma-delta modulation in mono-bit digital receivers for ultra-wideband communications," in *Proc. UWBST 2003, IEEE Conf. Ultra Wideband Systems and Technologies*, Reston, VA, Nov. 2003.
[13] S. Hoyos, B. M. Sadler, and G. R. Arce, "Mono-bit digital receivers for ultra-wideband communications," *IEEE Trans. Wireless Commun.,* to be published.
[14] S. R. Velazquez, T. Q. Nguyen, and S. R. Broadstone, "Design of hybrid filter banks for analog/digital conversion," *IEEE Trans. Signal Process.*, vol. 4, pp. 956–967, Apr. 1998.
[15] J. Franca, A. Petraglia, and S. K. Mitra, "Multirate analog-digital systems for signal processing and conversion," *Proc. IEEE*, vol. 85, no. 2, pp. 242–262, Feb. 1997.
[16] W. Namgoong, "A channelized digital ultra-wideband receiver," *IEEE Trans. Wireless Commun.*, vol. 3, pp. 502–510, May 2003.
[17] A. Petraglia and S. Mitra, "Analysis of mismatch effects among A/D converters in time-interleaved waveform digitizer," *IEEE Trans. Intstrum. Meas.*, vol. 40, pp. 831–835, Oct. 1991.
[18] R. Khoini-Poorard, "Mismatch effects in time-interleaved oversampling converters," in *Proc. IEEE Int. Symp. Circuits Systems*, London, U.K., May 1994, pp. 429–432.
[19] S. Hoyos, B. M. Sadler, and G. R. Arce, "Analog to digital conversion of ultra-wideband signals in orthogonal spaces," in *Proc. UWBST 2003, IEEE Conf. Ultra Wideband Systems and Technologies*, Reston, VA, Nov. 2003.
[20] S. Hoyos, B. M. Sadler, and G. R. Arce, "High-speed A/D conversion for ultra-wideband signals based on signal projection over basis functions," in *Proc. ICASSP 2004, Int. Conf. Acoustics, Speech and Signal Process.*, Montreal, Quebec, Canada, 2004.
[21] H.-J. Lee, D. S. Ha, and H.-S. Lee, "A frequency-domain approach for all-digital CMOS ultra-wideband receivers," in *Proc. UWBST 2003, IEEE Conf. Ultra Wideband Systems and Technologies*, Reston, VA, Nov. 2003.
[22] A. Papoulis, "Generalized sampling expansion," *IEEE Trans. Circuits Syst.*, vol. CAS-24, no. 11, pp. 652–654, Nov. 1977.
[23] Z. Cvetković, "Resilience properties of redundant expansions under additive noise and quantization," *IEEE Trans. Inf. Theory*, vol. 49, pp. 644–656, Mar. 2003.
[24] B. Beferull-Lozano and A. Ortega, "Efficient quantization for overcomple expansions in $\mathcal{R}^n$," *IEEE Trans. Inf. Theory*, vol. 49, pp. 129–150, Jan. 2003.
[25] N. T. Thao and M. Vetterli, "Reduction of the MSE in R-times oversampled A/D conversion from $\mathcal{O}(1/R)$ to $\mathcal{O}(1/R^2)$," *IEEE Trans. Signal Process.*, vol. 42, pp. 200–2003, Jan. 1994.
[26] N. T. Thao and M. Vetterli, "Deterministic analysis of oversampled A/D conversion and decoding improvements based on consistent estimates," *IEEE Trans. Signal Process.*, vol. 42, pp. 519–531, Mar. 1994.
[27] A. Gersho and R. M. Gray, *Vector Quantization and Signal Compression*. Boston, MA: Kluwer, 1992.
[28] T. M. Cover and J. A. Thomas, *Elements of Information Theory*. New York: Wiley, 1991.
[29] Y. Wang, J. Ostermannn, and Y. Zhang, *Video Processing and Communications*. Upper Saddle River, NJ: Prentice Hall, 2002.
[30] V. Trees, *Detection, Estimation, and Modulation Theory*. New York: Wiley, 2001.
[31] S. Haykin, *Adaptive Filter Theory*, 4th ed. Upper Saddle River, NJ: Prentice-Hall, 2002.
[32] A. V. Oppenheim and R. W. Shafer, *Discrete-Time Signal Process.*, 1st ed. Englewood Cliffs, N.J.: Prentice-Hall, 1989.
[33] S. Hoyos, B. M. Sadler, and G. R. Arce, "Broadband multicarrier communications receiver based on analog to digital conversion in the frequency domain," *IEEE Trans. Wireless Commun.,* to be published.
[34] A. Batra *et al.*, *Multi-Band OFDM Physical Layer Proposal for IEEE 802.15 Task Group 3a*,, Sep. 2003.
[35] H. F. Harmuth, *Transmission of Information by Orthogonal Functions*, 2nd ed. New York: Spring-Verlag, 1971.
[36] L. R. Welch, "Walsh functions and Hadamard matrices," in *Proc. Walsh Functions Symposium*, 1971, pp. 163–165.
[37] J. L. Walsh, "A closed set of orthogonal functions," *Amer. J. Math.*, vol. 45, pp. 5–24, 1923.
[38] P. S. Moharir, K. R. Sama, and B. Prasada, "Walsh functions and Hadamard matrices," in *Proc. Walsh Functions Symposium*, 1971, pp. 142–150.
[39] M. Vetterli and J. Kovačević, *Wavelets and Subband Coding*. Englewood Cliffs, NJ: Prentice-Hall, 1995.

Sebastian Hoyos (M'03) was born in Cali, Colombia, in 1975. He received the B.S. degree from the Pontificia Universidad Javeriana (PUJ), Bogota, Colombia, in 2000, and the M.S. and Ph.D. degrees in electrical engineering from the University of Delaware, Newark DE, in 2002 and 2004, respectively.

He worked for Lucent Technologies Inc. from 1999 to 2000 as Technical Manager and Sales Engineer for the Andean region in South America. Simultaneously, he was an Adjunct Professor at the PUJ University, where he lectured on microelectronics and control theory. In the Fall of 2000, he enrolled in the Department of Electrical and Computer Engineering at University of Delaware. During his M.S. and Ph.D. studies, he worked under the PMC-Sierra Inc., Delaware Research Partnership Program, and the Army Research Laboratory (ARL) Collaborative Technology Alliance (CTA) in Communications and Networks. In the Fall of 2004, he joined the Department of Electrical Engineering and Computer Sciences at the University of California, Berkeley, where he is currently a Postdoctoral Researcher at the Berkeley Wireless Research Center. He has carried out industrial consulting with Conexant Systems Inc., Red Bank, NJ.

His research interests include communication systems, wireless communications, sensor network processing, robust signal processing, and mixed-signal high-speed processing and circuit design.

Brian M. Sadler (S'81–M'85–SM'00) received the B.S. and M.S. degrees from the University of Maryland, College Park, and the Ph.D. degree from the University of Virginia, Charlottesville, all in electrical engineering.

He is a Senior Research Scientist at the Army Research Laboratory (ARL) in Adelphi, MD. He was a Lecturer at the University of Maryland, and has been lecturing at The Johns Hopkins University since 1994 on statistical signal processing and communications.

Dr. Sadler is a Senior Editor for the IEEE Signal Processing Letters, was an Associate Editor for the IEEE TRANSACTIONS ON SIGNAL PROCESSING, is on the editorial board for the EURASIP Journal on Wireless Communications and Networking, and was a Guest Editor for the IEEE JOURNAL ON SELECTED AREAS IN COMMUNICATIONS special issue on Military Communications. He is a member of the IEEE TECHNICAL COMMITTEE ON SIGNAL PROCESSING FOR COMMUNICATIONS, and co-chaired the 2nd IEEE WORKSHOP ON SIGNAL PROCESSING ADVANCES IN WIRELESS COMMUNICATIONS (SPAWC-99). His research interests include signal processing for mobile wireless and ultra-wideband systems, and sensor signal processing and networking.